# A New Method to Compare Hourly Rainfall between Station Observations and Satellite Products over Central–Eastern China

CHEN Haoming[1*] (陈昊明), YU Rucong[1] (宇如聪), and SHEN Yan[2] (沈 艳)

1 *State Key Laboratory of Severe Weather, Chinese Academy of Meteorological Sciences, Beijing* 100081

2 *National Meteorological Information Center, Beijing* 100081

(Received January 19, 2016; in final form June 20, 2016)

**ABSTRACT**

This study employs a newly defined regional-rainfall-event (RRE) concept to compare the hourly characteristics of warm-season (May–September) rainfall among rain gauge observations, China merged hourly precipitation analysis (CMPA-Hourly), and two commonly used satellite products (TRMM 3B42 and CMORPH). By considering the rainfall characteristics in a given limited area rather than a single point or grid, this method largely eliminates the differences in rainfall characteristics among different observations or measurements over central–eastern China. The results show that the spatial distribution and diurnal variation of RRE frequency and intensity are quite consistent among different datasets, and the performance of CMPA-Hourly is better than the satellite products when compared with station observations. A regional rainfall coefficient (RRC), which can be used to classify local rain and regional rain, is employed to represent the spatial spread of rainfall in the limited region defining the RRE. It is found that rainfall spread in the selected grid box is more uniform during the nocturnal to morning hours over central–eastern China. The RRC tends to reach its diurnal maximum several hours after the RRE intensity peaks, implying an intermediate transition stage from convective to stratiform rainfall. In the afternoon, the RRC reaches its minimum, implying the dominance of local convections on small spatial scale in those hours, which could cause large differences in rain gauge and satellite observations. Since the RRE method reflects the overall features of rainfall in a limited region rather than at a fixed point or in a single grid, the widely recognized overestimation of afternoon rainfall in satellite products is not obvious, and thus the satellite estimates are more reliable in representing sub-daily variation of rainfall from the RRE perspective. This study proposes a reasonable method to compare satellite products with rain gauge observations on the sub-daily scale, which also has great potential to be used in evaluating the spatiotemporal variation of cloud and rainfall in numerical models.

**Key words:** regional rainfall event, regional rainfall coefficient, diurnal variation, spatial spread, satellite precipitation

**Citation:** Chen Haoming, Yu Rucong, and Shen Yan, 2016: A new method to compare hourly rainfall between station observations and satellite products over central–eastern China. *J. Meteor. Res.*, **30**(5), 737–757, doi: 10.1007/s13351-016-6002-5.

## 1. Introduction

Because of its nonhomogenous behavior in terms of event occurrence and intensity, rainfall is one of the most important and challenging meteorological variables. The spatial and temporal distributions of rainfall are closely related to drought, river runoff, and soil erosion, which usually cause negative environmental and social consequences (Houze Jr., 1997; Carbone et al., 2002; Trenberth et al., 2003; Zhang and Zhai, 2011; Chen Jiong et al., 2013; Moseley et al., 2013). Understanding the structure and variation of precipitation is fundamental in meteorology. In particular, detailed knowledge regarding rainfall characteristics is particularly important in the validation of numerical models. Specifically, the diurnal variation of rainfall is fundamental to regional climate, and provides more information on the nature and characteristics of pre-

Supported by the Outstanding Tutors for Doctoral Dissertations of S & T Project in Beijing (20138005801), National Natural Science Foundation of China (41375004), and Basic Scientific Research and Operation Foundation of the Chinese Academy of Meteorological Sciences (2014R013).

*Corresponding author: chenhm@camscma.cn.

cipitation (Tren-berth et al., 2003; Dai et al., 2007; Yu et al., 2010; Yuan et al., 2010; Li et al., 2011; Yu and Li, 2012). The regional and global features of rainfall diurnal variations have been extensively studied with ground-based meteorological observations (Wallace, 1975; Dai et al., 1999; Yu et al., 2007b), precipitation radar (Nesbitt and Zipser, 2003; Bhatt and Nakamura, 2005; Bowman et al., 2005), and meteorological satellites carrying infrared radiometers (Yang and Slingo, 2001) or microwave radiometers (Sorooshian et al., 2002). Owing to certain types of spatial or temporal sampling limitations of in-situ datasets, more studies on the diurnal cycle of precipitation are based on satellite observations—especially those products deemed to be of high-quality, uniform, and consistent, such as the Tropical Rainfall Measuring Mission (TRMM) (e.g., Bowman et al., 2005; Hirose and Nakamura, 2005; Chen G. X. et al., 2013; Satoh and Kitao, 2013; Xu, 2013) and the NOAA Climate Prediction Center Morphing Technique (CMORPH) (e.g., Janowiak et al., 2005; Bao and Zhang, 2013; Guo et al., 2014).

However, previous studies have indicated that there is considerable uncertainty when applying radiometer-sensed satellite products to diurnal variations. It is widely recognized that afternoon and evening rainfall in satellite products tends to shift a few hours later than that in surface observations over land areas (Dai et al., 2007; Huffman et al., 2007; Kikuchi and Wang, 2008; Sapiano and Arkin, 2009), resulting in overestimation of rainfall during the afternoon and underestimation of rainfall during the late night and morning in satellite estimates (Sorooshian et al., 2002). Zhou et al. (2008) compared the diurnal cycle of the East Asian summer monsoon rainfall among rain gauge observations and two satellite estimates, and pointed out that the satellite products overestimated the rainfall frequency but underestimated its intensity over eastern China. Meanwhile, both satellite products overestimated the afternoon rainfall peak, especially in the regions between the Yangtze and Yellow rivers, with a robust semi-diurnal variation. Similarly, Shen et al. (2010) noted that the early morning (afternoon) rainfall peak associated with the Meiyu rainbelt over central–eastern China was substantially underestimated (overestimated) in six high-resolution satellite precipitation products. Yuan et al. (2012) investigated the sources of the differences between gauge measurements and TRMM products. They concluded that the overestimation of afternoon rainfall in TRMM, including the enhanced rainfall in TRMM when both datasets measured the rainfall but light rainfall was detected only by TRMM, strengthened in the afternoon rainfall amount and frequency.

Previous studies have mostly compared satellite products with rain gauge measurements at the gauge locations (e.g., Bowman et al., 2005; Chen Haoming et al., 2012; Yuan et al., 2012), or by interpolating the different datasets to the same resolution (e.g., Zhou et al., 2008). This approach is not entirely reasonable because rainfall events usually demonstrate considerable spatiotemporal inhomogeneity, and the retrieval algorithms are completely different between rain gauge measurements and satellite estimates. Moreover, algorithms vary even more among satellite products. A rain gauge measures accurate surface precipitation at a fixed location, but it fails to represent precipitation with high spatial variation, especially over regions over complex terrain (Ciach, 2003). Satellite precipitation products are able to detect spatial and temporal variations of precipitation at a finer resolution. However, satellite-based remote sensing is an indirect estimation of precipitation, which contains regional and temporal systematic biases and random errors (Shen et al., 2010, 2014; Tian et al., 2010). Point-to-point comparison or simple interpolation could inherently cause the biases for satellite products.

In addition, previous comparison studies have mainly focused on the temporal variation of rainfall at one location or in one grid, with the spatial variation rarely being considered. Rainfall events usually show great spatial and temporal inhomogeneity, and these variabilities in space and time are not independent of one another (Soltani and Modarres, 2006; Moron et al., 2010; Moseley et al., 2013). Toews et al. (2009) suggested that local and regional precipitation events contribute differently to groundwater processes, and they also mentioned that the ability to predict lo-

cal precipitation is rather poor in current global climate models. Regional rain is usually closely related to mesoscale systems, while local rain is more closely related to isolated convections. The abilities of different measurements in detecting local and regional rain could be an important cause of the differences between in-situ observations and satellite-based remote sensing. The detection ability of widely-spread regional rain could be equivalent between a rain gauge at a fixed location and satellite-based remote sensors, while that of local rain with limited spatial spread could be very different.

Recently, Yu et al. (2015) defined a new regional-rainfall-event (RRE) concept to study the spatiotemporal variation of rainfall over a limited area, and they also defined a new regional rainfall coefficient (RRC) to classify local rain and regional rain in a given area. They showed that the RRC, together with intensity and duration, provides more information on the complete spatiotemporal organization and evolution of RREs, which are defined by observed rainfall at multiple, well-distributed stations in a limited area. The definition of an RRE reflects the regional mean characteristics of rainfall events. In terms of the regional mean state in a limited area, the rain gauge observations and satellite-based remote sensing measurements could have comparable ability in detecting rainfall events. Thus, RREs are more suitable for comparison between different datasets.

In this study, the newly defined RRE concept of Yu et al. (2015) is employed to compare warm season (May–September) hourly rainfall characteristics between gauge measurements and satellite precipitation products. The newly released China merged hourly precipitation analysis (CMPA-Hourly), which is a combination of station and satellite observations, is also used, and we evaluate its performance in representing the hourly rainfall features over central–eastern China. The results will be a useful reference for the use of high-resolution satellite precipitation products in analyzing sub-daily rainfall features. Furthermore, the method may also have great potential in evaluating the spatiotemporal variation of cloud and rainfall in numerical models. Following this introduction, Section 2 describes the rainfall datasets and defines the RRE. The mean frequency, intensity, and regional differences of the RRE are presented in Section 3. Section 4 examines the diurnal variation of the RRE and corresponding variation of the RRC. Concluding remarks are given in Section 5.

## 2. Data and methods

### *2.1 Data description*

This study uses the hourly rainfall records of more than 10000 automatic weather stations over central–eastern China (18°–43°N, 100°–125°E) in the warm season (May–September) during 2008–2013. The gauge-observed hourly rain data were obtained from the national climatic reference network, the national weather surface network, and regional automatic weather stations. The dataset was collected and quality-controlled by the National Meteorological Information Center (NMIC) of the China Meteorological Administration (CMA). The black dots in Fig. 1 mark the locations of the stations.

The hourly, 0.1° × 0.1°, merged precipitation analysis product, CMPA-Hourly (Shen et al., 2014),

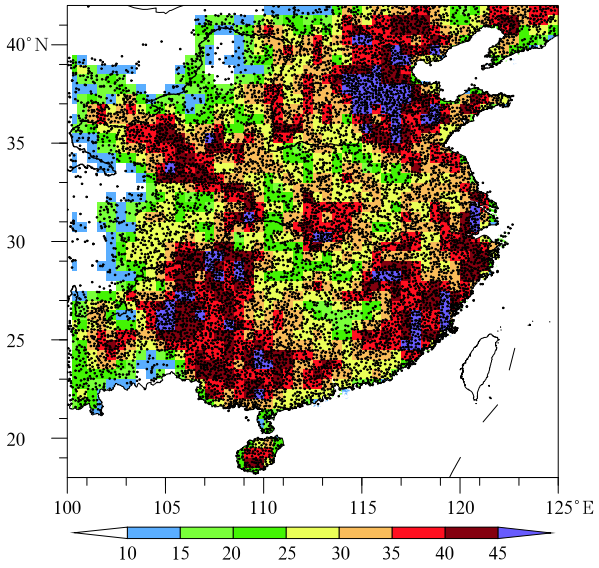


**Fig. 1.** Locations of the automatic weather stations (black dots) over central–eastern China. Color shading denotes the number of stations on each 0.5° grid used in this study.

from 2008 to 2013, was also provided by the NMIC of the CMA. The CMPA-Hourly merges high-density hourly data from automatic weather stations over China with the CMORPH precipitation product by using the improved Probability Density Function and Optimal Interpolation (PDF-OI) merging algorithm. Over central–eastern China, with its high density of stations, CMPA-Hourly data mainly reflect the rainfall characteristics of these stations, and the satellite estimates do not evidently influence the data quality over this region. However, due to the effect of interpolation, the finer detail of the rainfall characteristics in CMPA-Hourly grids may still differ from that at the rain gauge stations around the grids. A report on the overall quality of CMPA-Hourly and its cross-validation results with station records can be found in Shen et al. (2014). The real-time data are provided on the NMIC website: http://cdc.nmic.cn/sksj.do?method=ssrjscprh.

To further reveal the reliability of satellite-based estimates on the sub-daily scale, two satellite precipitation products are used in this study. The first satellite product is TRMM 3B42 precipitation data (3 hourly, 0.25°) from 2008 to 2013 (Huffman et al., 2007). This product was derived by using an optimal combination of microwave rain estimates from TRMM, SSM/I (Special Sensor Microwave Imager), AMSU (Advanced Microwave Sounding Unit), and AMSR (Advanced Microwave Scanning Radiometer), to adjust infrared (IR) estimates from geostationary IR observations. In addition, the CMORPH product (3 hourly, 0.25°) from the same period is also used in this study (Joyce et al., 2004). CMORPH exclusively uses precipitation estimates derived from low orbiting satellite microwave observations, and the observational features are transported via spatial propagation information obtained entirely from the IR data of geostationary satellites.

### *2.2 Definition of RRE and RRC*

The definition of the RRE follows that of Yu et al. (2015), which considers the rainfall characteristics in a limited region as a whole to investigate the regional rainfall distribution and evolution. Since Yu et al. (2015) focused on a small region over the Beijing plain, they defined the RRE by observed rainfall at only eight stations, well-distributed over the selected region. In this study, we extend the limited region to a large area over central–eastern China. Due to considerable inhomogeneity in the rainfall distribution, the RRE still needs to be defined in a limited area to effectively represent the overall features of rainfall in the selected region. Here, a 0.5° scan radius is used to define the RRE. This means that the rainfall occurring in a 0.5° × 0.5° grid box is considered as a whole, which is represented by the definition of the RRE. The scan radius is alterable according to the region of interest. In this study, as the horizontal resolutions of TRMM and CMORPH are both 0.25°, a smaller scan radius would not be able to provide enough samples in the grid box for the two satellite products. A 1° scan radius was also tested, and the results showed no qualitative differences to those described below. After determining the scan radius, the area covering central–eastern China is divided into 51 × 51 grid boxes with 0.5° intervals. In each grid box, the $N$ records from all stations or satellite grids are composited to define the RRE. The number of samples $N$ is different for stations and satellite products. For stations, the number of stations in each grid box is shown by color shading in Fig. 1. In most of central–eastern China, there are more than 15 stations in each grid box; only in some western regions is the number relatively smaller. As indicated by Yu et al. (2015), the composite should be suitable to any limited region with $N \geqslant 3$ stations. For gridded data, $N$ is equal in all grid boxes, e.g., $N = 25$ for CMPA-Hourly and $N = 4$ for both TRMM and CMORPH.

For each hour $t$, the maximum record $P_{xt} = \max(P_{it})(i = 1, ..., N)$ is defined, where $P_{it}$ is the measurable rainfall ($\geqslant 0.1$ mm h$^{-1}$) at the station or grid $i$ in each grid box. The time series of $P_{xt}$ are then used to represent the rainfall intensity at hour $t$ over the grid box. It is worth noting that $P_{xt}$ is used as an index to represent RRE because the regional rainfall intensity can be well represented (please also see Fig. 3a in Yu et al. (2015)). However, the RRE is a more

generalized concept, and other indexes can also be used to represent its features. For example, the hourly mean rainfall intensity, $P_{mt} = \frac{1}{N}\sum_{i=1}^{N} P_{it}$, at hour $t$, was also tested. The results were similar to those using $P_{xt}$ while using the time series of $P_{mt}$. In the following analyses, the time series of $P_{xt}$ are used to define RREs. The durational features, which are defined by hours without any intermittence or at most 1-h intermittence during a single event, are also investigated, following Yu et al. (2007a).

The RRC defined by Yu et al. (2015) is used to quantify the rainfall spatial variability in the grid box defining the RRE. For each hour with measurable rainfall (i.e., from the beginning hour $t_1$ to the end hour $t_2$), the hourly rainfall intensity $P_{it}$ at each hour $t$ is reordered from the largest $P_{1t}$ to the smallest $P_{N_at}$, i.e., $P_{1t} \geqslant P_{2t} \geqslant ... \geqslant P_{N_at} \geqslant 0.01$ mm h$^{-1}$. Then, the RRC is defined as

$$\mathrm{RRC} = \frac{2P_{mn}}{P_{1t} + P_{N_at}} \times \frac{N_a - 1}{N - 1}, \tag{1}$$

where $P_{mn} = \frac{1}{N_a}\sum_{i=1}^{N_a} P_{it}$, $N$ is the number of samples in each grid box at the hour $t$, and $N_a$ represents the number of stations or grids that have measureable rainfall. For a grid box with no rainfall, the RRC in the grid box will not be calculated. The first item of the RRC equation presents the homogeneity of the rainfall intensity distribution in the given grid box. As $P_{it}$ is a monotonically decreasing permutation, the first item of the equation implies that if more than half of the stations or grids have rainfall stronger than the mean intensity $P_{mn}$, the RRC could be large, indicative of a regional event. The second item of the equation involves the number of stations or grids that can be regarded as rainy ones in the area. Generally, the RRC can be used to separate local rain and regional rain. For local rain with small scale, the RRC is smaller; for regional rain more uniformly spread over the selected grid box, the RRC is larger.

Due to limitations regarding the sensitivity of tipping-bucket rain gauge instruments in China, hours with rainfall intensity less than 0.1 mm are considered non-rain hours in the gauge observations. In the following analyses, only hours with rainfall intensity greater than 0.1 mm h$^{-1}$ are treated as rainy hours for all four datasets. For each hour and in each grid box, the warm season means of RRE frequency (defined as the percentage of hours having measurable precipitation, i.e., $F_h = \frac{N_{Ph}}{N_{Sh}}$, where $F_h$ is the RRE frequency in hour $h$ during the day, $N_{Ph}$ is the number of days with measurable precipitation, and $N_{Sh}$ is the number of days with observational records in hour $h$) and intensity (the mean rates averaged over the precipitating hours, i.e., $I_h = \frac{A_h}{N_{Ph}}$, where $I_h$ is the intensity of the RRE in hour $h$, and $A_h$ is the measurable rainfall amount) are calculated for each year. The multi-year (2008–2013) mean of warm season precipitation quantities are derived by averaging the hourly or 3-hourly quantities for each dataset. A composite diurnal cycle of these precipitation quantities is derived from averaging the hourly data over the years.

## 3. Mean state of the RRC, as well as the frequency and intensity of RREs

One of the causes of the differences between rain gauge observations and satellite data is that the former are obtained at a fixed location while the latter are retrieved in a relative coarse grid. For the CMPA-Hourly dataset, which combines rain gauge observations with high-resolution satellite estimations, its difference with gauge observations in terms of diurnal variation has not previously been revealed. To evaluate the performance of CMPA-Hourly data, as well as illustrate the common biases of satellite data on the sub-daily timescale, the diurnal phases of warm-season rainfall frequency from rain gauge observations, CMPA-Hourly, TRMM, and CMORPH, are compared in Fig. 2. Consistent with the previous studies (Yu et al., 2007b; Zhou et al., 2008; Yuan et al., 2012), in the rain gauge measurements (Fig. 2a), the afternoon peak is obvious in southeastern coastal regions. In the northern regions, the number of stations with an afternoon peak is comparable to that with a nocturnal peak. In the west of central–eastern China, nocturnal to morning peaks dominate the diurnal variation of the warm-season rainfall frequency. The diurnal vari-

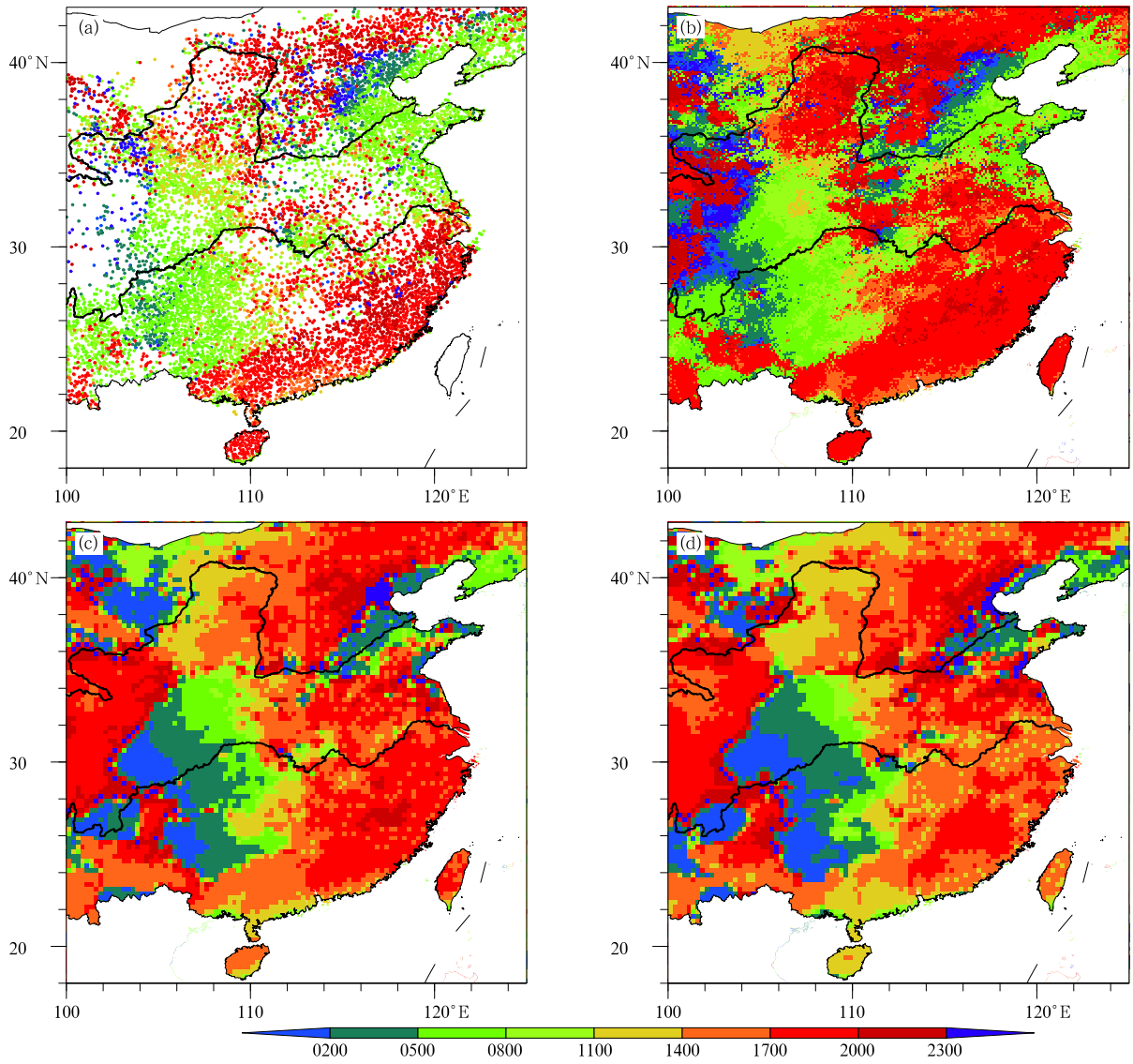


**Fig. 2.** Spatial distributions of the diurnal phase (Local Solar Time; LST) of the 2008–2013 warm-season (May–September) mean hourly rainfall frequency from (a) rain gauges, (b) CMPA-Hourly, (c) TRMM, and (d) CMORPH products. The different colors represent different hours. The Yellow and Yangtze rivers are marked by thick black lines.

ation of rainfall frequency in the CMPA-Hourly data is quite similar to that over the gauge observations, especially over regions with a high density of stations (Fig. 2b). The nocturnal peak over the east of Tibet, the morning peak over the middle reaches of the Yangtze River valley, and the afternoon peak in southeastern regions, are well represented. However, over regions with a relatively sparse distribution of stations, especially over the middle reaches of the Yangtze River and regions between the Yangtze and Yellow rivers, where semi-diurnal variation is obvious, the CMPA-Hourly data tend to overestimate the afternoon peak, possibly because of the biases introduced by the CMORPH data. The overestimation of the afternoon frequency peak is more evident in the TRMM and CMORPH data (Figs. 2c and 2d). In these two satellite estimates, the afternoon peak dominates the regions east of 110°E.

The biases of satellite data on the sub-daily scale, even the CMPA-Hourly data, may introduce a number of uncertainties in analyzing the features of hourly rainfall. However, these data are essential in such anal-

yses because of the limitations of the rain gauge distribution. It is noted that the evaluation could be unfair for satellite estimates, because the station gauges only observe the rainfall at a fixed location, whereas satellite-based rainfall is more likely to be an average of a grid. In the following analyses, it is illustrated that, by defining the RRE, such a comparison could become more reasonable, largely eliminating the difference caused by the observational measurements among different datasets.

The RRC indicates the spatial spread of the rain in a given grid box. The warm-season mean RRC from four datasets is shown in Fig. 3. The values among the datasets are different, because they depend greatly on the number of samples in each grid box (i.e., $N$) in Eq. (1). The values in CMPA-Hourly (Fig. 3b) are larger than those in the gauge measurements (Fig. 3a), and are even larger in the TRMM (Fig. 3c) and

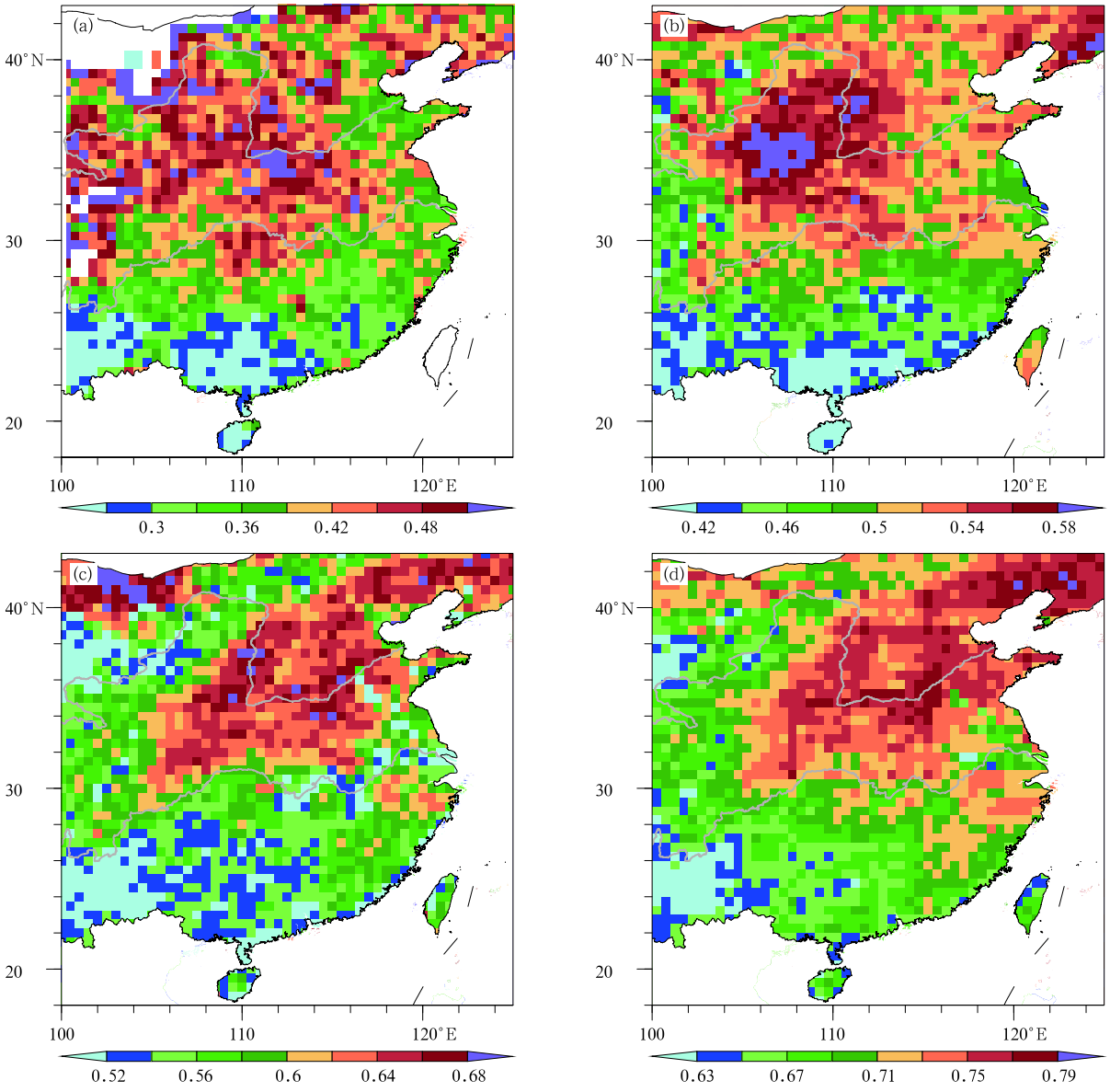


**Fig. 3.** Spatial distributions of 2008–2013 warm-season mean RRC in each 0.5° grid derived from (a) rain gauge observations, (b) CMPA-Hourly, (c) TRMM, and (d) CMORPH. The Yellow and Yangtze rivers are marked by white lines.

CMORPH (Fig. 3d) products. Nevertheless, all four datasets show similar spatial distributions of warm-season RRC over central–eastern China. The pattern correlation coefficients between station observations and the other three data all reach 0.98. The root-mean-square error (RMSE) of CMPA-Hourly is 0.12, smaller than those of TRMM and CMORPH (Table 1). The RRC is smaller over the south of the Yangtze River valley, implying more local convection over these regions. In the regions north of 30°N, the RRC is larger than that in the southern regions. Furthermore, the largest RRC appears over the Hetao region. This large-value center is evident in both rain gauge observations and CMPA-Hourly; while in TRMM and CMORPH, the value of the RRC over the Hetao region is similar to that in northern China. Over the eastern slope of the Tibetan Plateau, the RRC in rain gauge observations is larger than that in the other three datasets, which could be largely due to the sparse distribution of stations over this region (Fig. 1). This to some extent implies that the definition of the RRE should be more reliable in regions with a dense observational network that uses gauge records.

The consistency in the mean RRC spatial distribution indicates that the application of the RRE method to analyze hourly rainfall features is reliable. The warm-season mean RRE frequencies are then compared for the four datasets (Fig. 4). Generally,

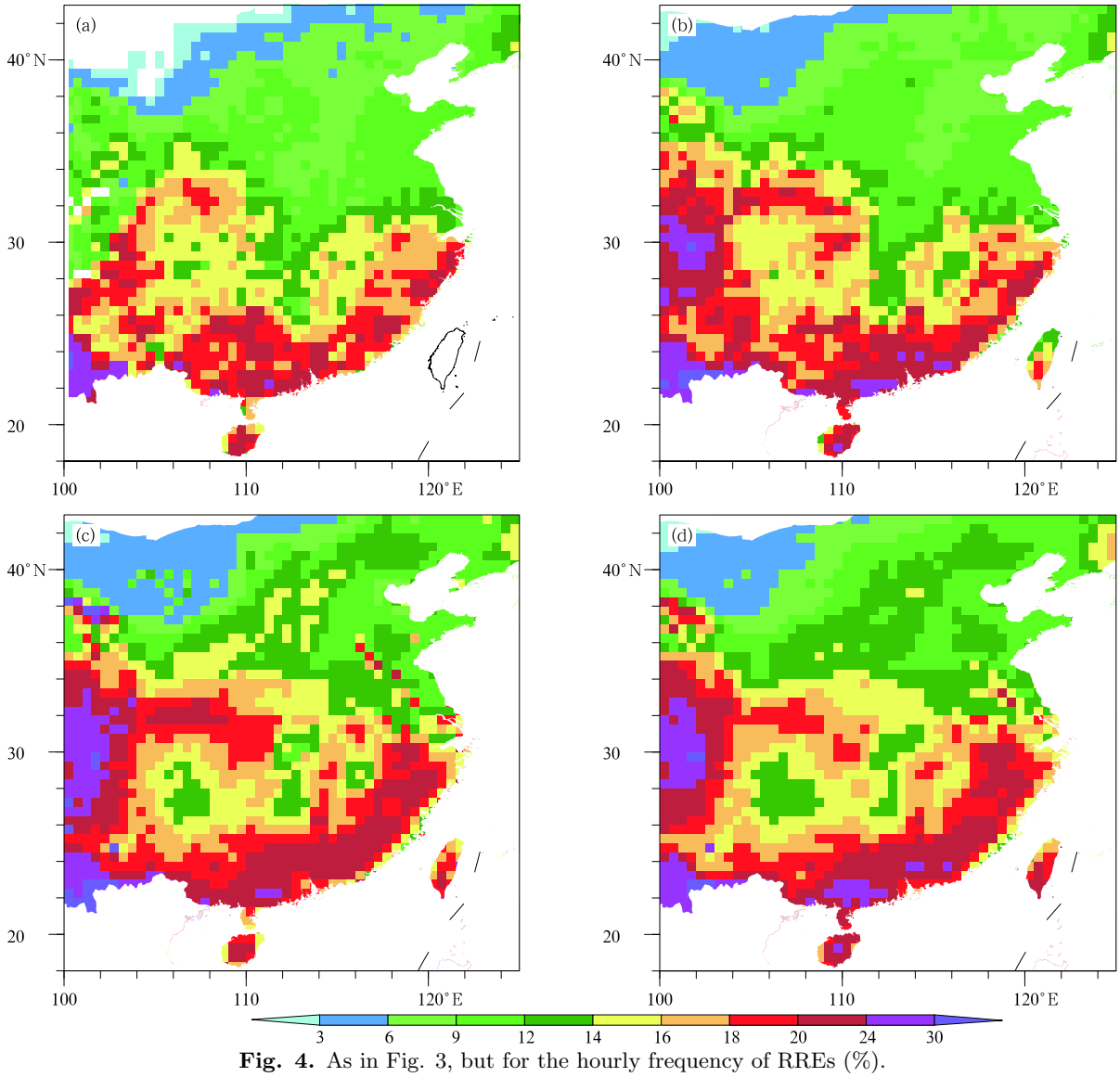


**Fig. 4.** As in Fig. 3, but for the hourly frequency of RREs (%).

the RRE frequencies are comparable among the four datasets. It is clear that the overestimation of frequency in satellite-based products is largely eliminated when compared by using the RRE method. Consistent with previous studies (Zhou et al., 2008), the frequency patterns derived from both satellite products are reasonably realistic. The spatial pattern is closer to surface observations in CMPA-Hourly than in TRMM and CMORPH. The pattern correlation coefficients between station observations and the other three datasets all exceed 0.96 (Table 1). The RMSE of CMPA-Hourly is 3.47%, also smaller than TRMM (5.14%) and CMORPH (4.61%). RREs occur more frequently over regions south of the Yangtze River, where the RRC is relatively small; while in most of the northern regions, the warm-season RRE frequency is less than 16%. Over the Sichuan basin, the frequency reaches 16%–20% in all datasets. Also of note is that, over the eastern slope of the Tibetan Plateau, both CMPA-Hourly and the two satellite products show a larger frequency than surface observations. As mentioned above, there could be large uncertainties in regions with a sparse distribution of stations, even when using RREs to investigate hourly rainfall features among different datasets. Over the eastern slope of the Tibetan Plateau, with its steep topography, the number of stations in each grid box is smaller and their distribution is non-uniform (Fig. 1). Thus, the RRE features may not be fully captured by this limited number of stations in this area. Comparing CMPA-Hourly and CMORPH, the CMPA-Hourly data show evident advantages in terms of spatial distribution compared with the original satellite products (Table 1).

**Table 1.** Pattern correlation coefficients and RMSE between the station-observed, CMPA-Hourly, and satellite-derived RREs' RRC (Fig. 3), frequency (Fig. 4), and intensity (Fig. 5)

| Variable | Pattern correlation | | | RMSE | | |
|---|---|---|---|---|---|---|
| | CMPA-Hourly | TRMM | CMORPH | CMPA-Hourly | TRMM | CMORPH |
| RRC | 0.98 | 0.98 | 0.98 | 0.12 | 0.15 | 0.31 |
| Frequency (%) | 0.98 | 0.96 | 0.97 | 3.47 | 5.14 | 4.61 |
| Intensity (mm $h^{-1}$) | 0.99 | 0.98 | 0.98 | 0.2 | 0.35 | 0.27 |

The hourly intensity of RREs among the different datasets also presents a similar spatial pattern (Fig. 5). The hourly intensity is larger in the eastern regions than in the western regions. The maximum intensity reaches 1.2–1.6 mm $h^{-1}$ in the lower reaches of the Yangtze and Yellow rivers in station observations (Fig. 5a); and in most of the western regions, the RRE intensity is smaller than 1 mm $h^{-1}$. The intensity distribution in CMPA-Hourly is close to station observations (Fig. 5b). However, the intensity is slightly stronger over regions with relatively fewer stations, e.g., the middle reaches of the Yangtze River valley. The RRE intensity is also stronger in the Sichuan basin in CMPA-Hourly. TRMM (Fig. 5c) and CMORPH (Fig. 5d) reproduce the spatial distribution of warm-season RRE intensity, but the overestimation is more obvious in these two datasets, especially for TRMM. In most of the eastern regions, the RRE intensity is greater than 1.2 mm $h^{-1}$ in TRMM, which is 0.4–0.8 mm $h^{-1}$ larger than that in the other three datasets. Similar to the distribution of RRE frequency, the intensity of CMPA-Hourly is closer to station observations compared with CMORPH. Despite the differences in values, which could be caused by the inherent differences among datasets, the spatial distribution of both frequency and intensity is comparable, as the pattern correlation coefficients all exceed 0.98 (Table 1), implying that the RRE method is suitable for investigating the climatic distribution of rainfall features for different datasets.

## 4. Diurnal variation of warm-season RREs

### *4.1 Diurnal variation of RREs and its relationship with that of RRCs*

The above section shows that the spatial distributions of RRE frequency and intensity are quite consistent among rain gauge observations, CMPA-Hourly,

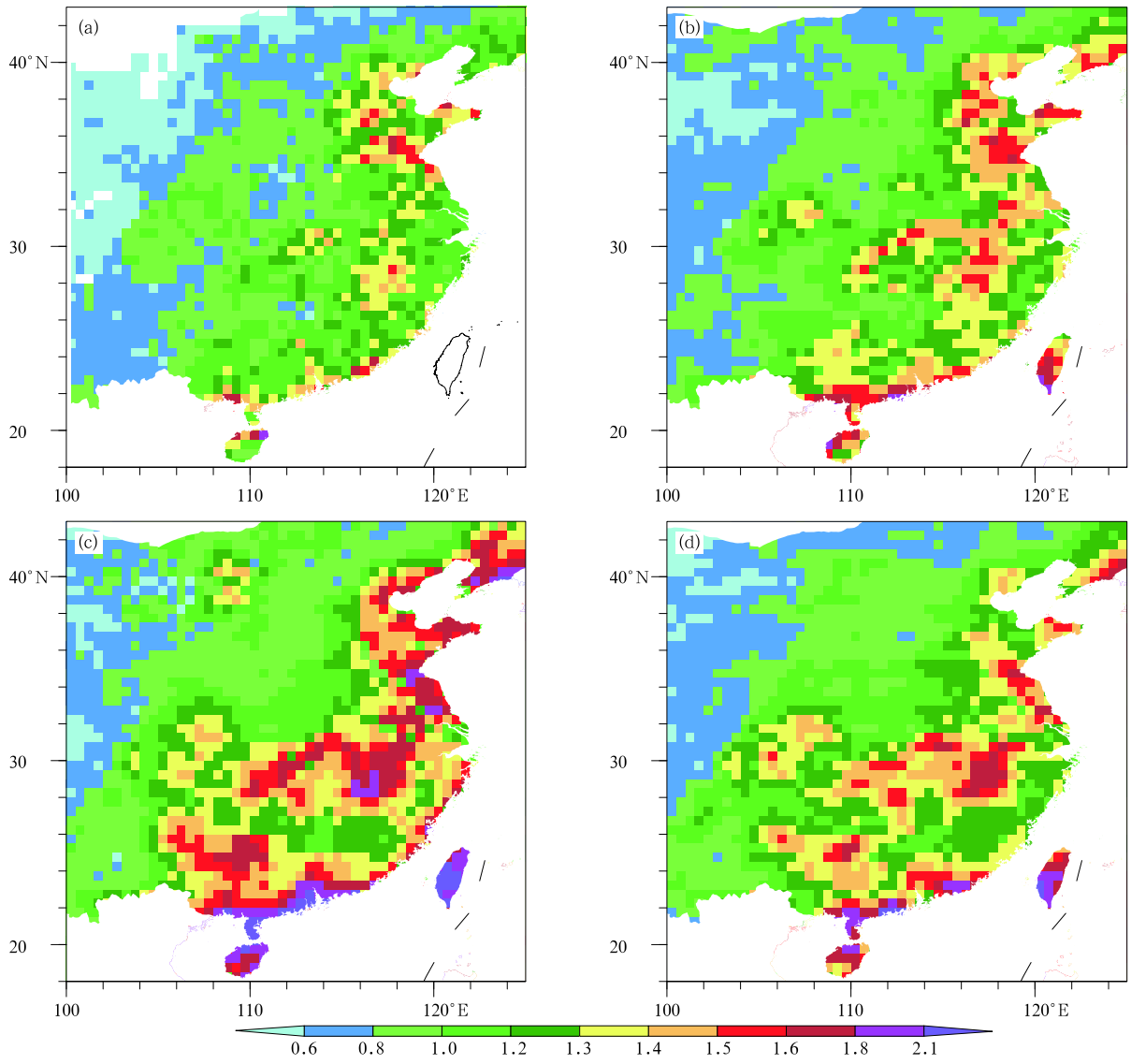


**Fig. 5.** As in Fig. 3, but for the hourly intensity of RREs (mm $h^{-1}$).

and the two satellite products. The diurnal variation of warm-season RREs is further analyzed in this section.

The diurnal phase, defined by the time of maximum during the day, for RRE intensity and frequency, is given in Fig. 6. The surface-observed diurnal phase of RRE intensity is similarly distributed to that using single station records (Fig. 6a). Distinct regional differences in the diurnal phase are seen over central–eastern China. Over the Sichuan basin, the RRE intensity tends to reach a peak in nocturnal hours, and the diurnal phase shows an evident eastward delay along the Yangtze River valley. Over southeastern China, the RRE intensity reaches a peak in the afternoon. Over the regions between the Yangtze and Yellow rivers, both morning and afternoon peaks are apparent, but the morning peak seems not as obvious as that in single station analyses. The morning peak is more evident in northern China.

The diurnal variation of RRE intensity in CMPA-Hourly is quite consistent with that in station observations (Fig. 6c). The nocturnal peak in southwestern and northern regions, afternoon peak in the southern region, and the double peaks between the Yangtze and

Yellow rivers, are all realistically reproduced. TRMM (Fig. 6e) and CMORPH (Fig. 6g) also represent the regional distribution of RRE intensity phase well, but they both show a timing of several hours earlier over most regions. For example, the RRE intensity reaches its diurnal peak at 0200 LST (Local Solar Time) in the Sichuan basin in both TRMM and CMORPH data, whereas it occurs at 0500 LST in surface observations and CMPA-Hourly data. In southern China, the shift in the diurnal phase is more obvious in CMORPH than

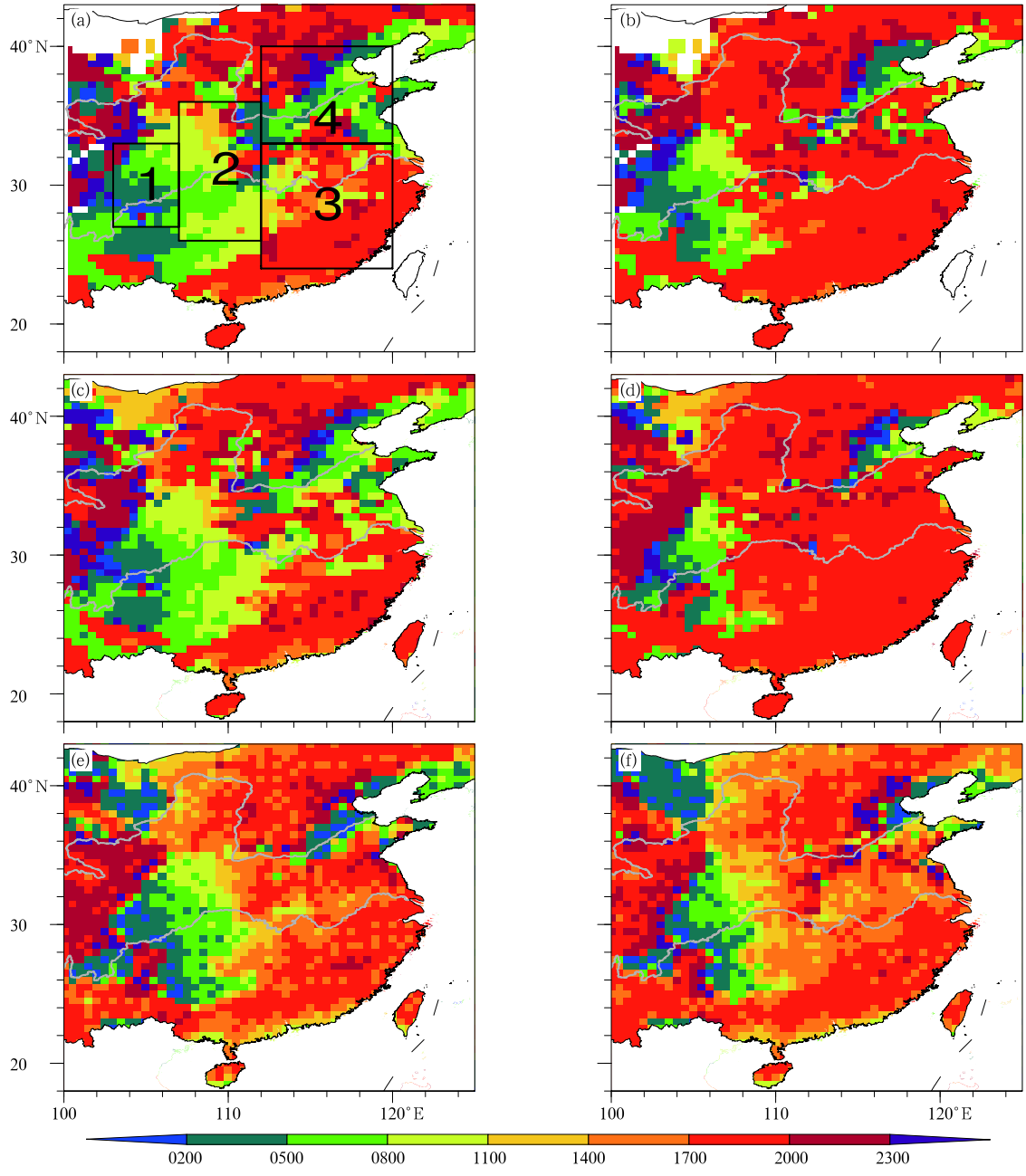


**Fig. 6.** The diurnal phases (LST) of the 2008–2013 warm-season (May–September) (a, c, e, g) mean intensity and (b, d, f, h) frequency of RREs from (a, b) rain gauges, (c, d) CMPA-Hourly, (e, f) TRMM, and (g, h) CMORPH. The different colors represent different hours. The Yellow and Yangtze rivers are marked by white lines. Four distinct regions are marked by rectangles in (a).

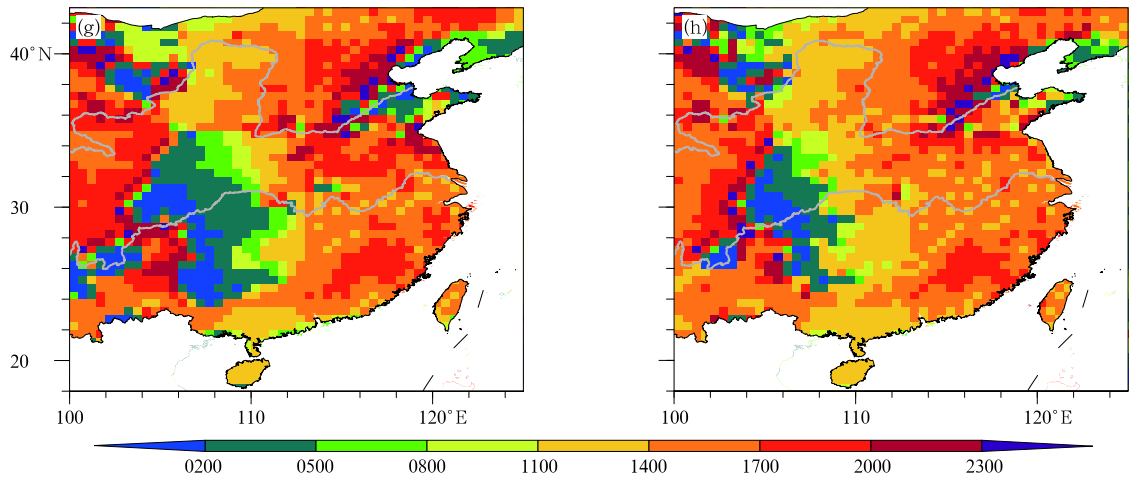


**Fig. 6.** (Continued.)

in TRMM. The morning peak over the regions between the Yangtze and Yellow rivers is not obvious in these two satellite datasets, but they reproduce the morning peak in northern China well.

The diurnal phases of RRE frequency are also compared (Figs. 6b, 6d, 6f, and 6h). Different from that of intensity, the RRE frequency reaches its peak during 1700–2000 LST over most of central–eastern China in surface observations (Fig. 6b). The nocturnal to morning peak is only obvious in the southwestern regions and coastal regions of northern China. The distribution of RRE frequency phase in CMPA-Hourly is consistent with that in surface observations. The TRMM and CMORPH data also present the dominant afternoon peaks over central–eastern China, albeit reaching them about 3 hours earlier. Considering the 3-h sampling of these two satellite products, the shift could be tolerable. In particular, the consistency in the mean frequency and diurnal phase of frequency indicates that the RRE method is reasonable for comparing sub-daily variations among different datasets.

To further illustrate the cause of the elimination of the differences, the diurnal phases of the RRC are presented in Fig. 7. Different from the diurnal phase of RRE frequency and intensity, the spatial distribution of RRC peak hours does not show uniform regional features in all datasets. The diurnal phases of the RRC in station observations (Fig. 7a) and CMPA-Hourly (Fig. 7b) show a similar pattern, except for the eastern slope of the Tibetan Plateau. Over the eastern slope of the Tibetan Plateau, where stations are relatively sparsely distributed, the rainfall information could be more contributed by CMORPH data in the CMPA-Hourly product. Furthermore, the differences between station observations and CMPA-Hourly over this region also imply an effect of sample number in a given area in calculating the RRC, which should be considered when applying the RRE method, especially over regions with steep topography. Over most regions of central–eastern China, both station observations and CMPA-Hourly show that the RRC reaches a diurnal peak during morning and noon. In southern regions, where the warm-season mean RRC is smaller, and in the Hetao region, where the mean RRC is largest, the RRCs tend to reach daily maximum during 0800–1400 LST. In the regions between the Yangtze and Yellow rivers, the peak hour is earlier, during 0200–0800 LST. The diurnal phases of the RRC in TRMM (Fig. 7c) and CMORPH (Fig. 7d) data are generally earlier than that in surface observations and CMPA-Hourly data, except over southern and central–eastern China. In these two regions, the RRC tends to reach its daily maximum in the afternoon, implying that satellite-based remote sensing is able to capture more organized rainfall systems in the afternoon. This is consistent with the overestimation of afternoon rainfall in the satellite products, as local rain tends to be distributed over the whole grid in the satellite data.

The regional mean diurnal cycles of the normal-

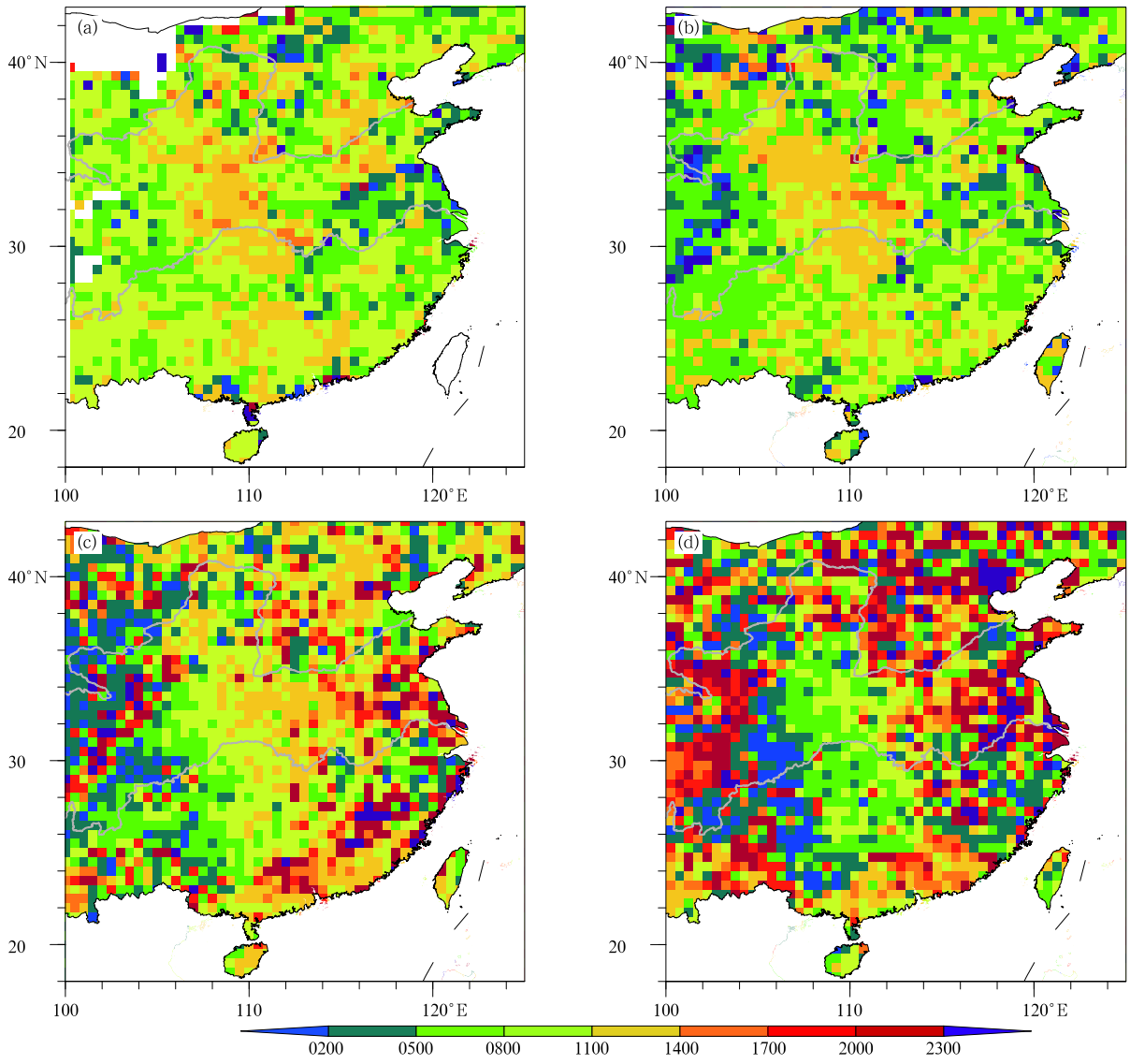


**Fig. 7.** The diurnal phases (LST) of the 2008–2013 warm-season RRC from (a) rain gauges, (b) CMPA-Hourly, (c) TRMM, and (d) CMORPH. The different colors represent different hours. The Yellow and Yangtze rivers are marked by gray lines.

ized RRC and RRE frequency and intensity are shown in Fig. 8. Four distinct regions (marked in Fig. 6a) are selected for comparison. Generally, the diurnal variations of the RRC and RRE frequency and intensity in CMPA-Hourly are all consistent with those in station observations. The TRMM and CMORPH products also show similar diurnal variation, albeit with a certain phase shift for the peak hours. An interesting phenomenon is that the RRC tends to reach its peak several hours after the RRE intensity reaches its peak, except in Region 3. In all regions, the RRC still increases after the RRE intensity reaches its peak and begins to decrease. The relationship between the evolution of the RRC and RRE intensity indicates that most RREs are uniformly spread to a larger area after reaching a peak. As the RRC represents the spatial spread of rain in a given box, a larger RRC indicates that the rain covers a larger area in the grid box. The lag in the RRC may imply an extension of the local convection system (with a smaller RRC but larger in-

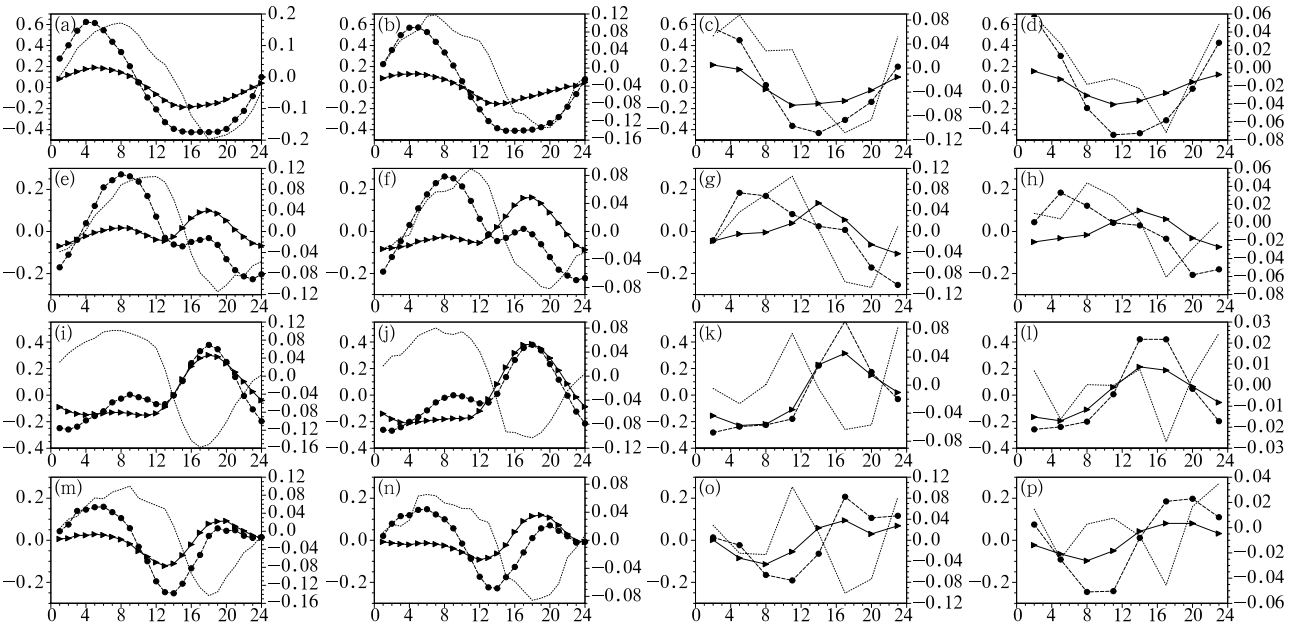


**Fig. 8.** Regional mean diurnal cycles of normalized (normalized by the daily mean) RRC (thin gray line; right $y$-axis), intensity (black line with dots; left $y$-axis) and frequency (black line with triangles; left $y$-axis) of RREs, averaged over the regions (a–d) 1, (e–h) 2, (i-l) 3, and (m–p) 4 as outlined in Fig. 6a, from (a, e, i, m) rain gauge measurements, (b, f, j, n) CMPA-Hourly, (c, g, k, o) TRMM, and (d, h, l, p) CMORPH.

tensity) to regional stratiform rainfall (with a larger RRC but weaker intensity), after its peak.

In Region 1, with a distinct nocturnal peak, both the rain gauge (Fig. 8a) and CMPA-Hourly (Fig. 8b) data show a large single peak around 0400 LST, and a valley at 1600 LST, in RRE intensity. The diurnal curve of RRE frequency is similar with that of intensity, but with a much weaker amplitude. The diurnal peak of the RRC occurs at 0800 (0700) LST for station (CMPA-Hourly) data, about 4 (3) h later than the peak hour of intensity. This signal is also evident in the TRMM data (Fig. 8c), but the diurnal phase shift is about 2–3 h, possibly because it is a 3-hourly dataset. For CMORPH data (Fig. 8d), the RRE frequency and intensity peaks are the same as in TRMM, but the RRC reaches its peak at the same time as that of RRE frequency and intensity.

In Region 2, where a near-noon peak of the RRC dominates (Fig. 7), the RRE intensity shows a strong morning peak in station (Fig. 8e) and CMPA-Hourly (Fig. 8f) data, and the frequency shows a strong afternoon peak. The peak hours are also the same for these two datasets. The RRC reaches its peak at 1200 LST, also 4 h later than that of intensity. The relationship between the diurnal variation of the RRC and RRE frequency is not clear. A shift in peak hours is also evident in TRMM (Fig. 8g) and CMORPH (Fig. 8h) data in Region 2. For example, the RRE intensity peaks at 0400 LST and the frequency peaks at 1300 LST, both 4–5 h earlier than that in station and CMPA-Hourly data. However, the lag in the RRC peak to that of intensity is reproduced well in both satellite products.

In Region 3, with a dominant afternoon peak for RRE intensity and frequency, both the RRE intensity and frequency show a large afternoon peak at 1800 LST in station (Fig. 8i) and CMPA-Hourly (Fig. 8j) data, and at 1700 LST in TRMM (Fig. 8k) and CMORPH (Fig. 8l) data. The RRC shows two comparable diurnal peaks, with a larger one in the morning and a smaller one around midnight. It seems that the dominant peak of the RRC is decoupled with the intensity peak in this region, which is quite different from the situation in the other regions. But, for the secondary peak, it still lags that of intensity by 6 h, which is evident in all datasets.

In Region 4, where the morning and afternoon peaks are both evident for RRE intensity (Fig. 6), the RRE intensity (frequency) reaches a dominant peak at 0600 (1800) LST in station (Fig. 8m) and CMPA-Hourly (Fig. 8n) data. The semi-diurnal variations of RRE frequency and intensity are also obvious in TRMM (Fig. 8o) and CMORPH (Fig. 8p) data, but the afternoon peak is stronger than the morning peak in the two satellite datasets. The RRC also shows remarkable semi-diurnal variation in all of the four datasets, with the two peaks both lagging those of intensity.

### *4.2 Diurnal variation of intense long-duration RREs in station observations and CMPA-Hourly data*

Previous results indicate that the CMPA-Hourly data perform much better than the two satellite datasets in revealing the mean state and diurnal variation of RREs. The durational features of RREs in CMPA-Hourly are further analyzed. As both TRMM and CMORPH are 3-hourly datasets, they are not used in the following analyses.

The mean durations of RREs from station observations and CMPA-Hourly data are compared in Fig. 9. The CMPA-Hourly (Fig. 9b) data show a consistent distribution of mean duration with station observations (Fig. 9a), with a pattern correlation coefficient of 0.99. The RREs in CMPA-Hourly tend to last longer than those in gauge observations, probably due to the effect of spatial interpolation. The RMSE for CMPA-Hourly is 2.72 h (Table 1). The regions with longer duration generally correspond to those with larger RRE frequency (Fig. 4). This is quite different to that based on a single station or grid, from which the regions with longer duration extend along the Yangtze River valley (Chen et al., 2010). This also implies inherent differences in the results by using a single station or grid and RREs. Because an RRE represents the mean rainfall characteristics of a limited region, the frequently occurring RRE could respond to longer duration. However, in single station or grid analyses, a longer duration usually corresponds to regions where the main rainbelt is located (Chen et al., 2010; Yuan et al., 2010).

The diurnal variation of RREs with different durations averaged over central–eastern China is illustrated in Fig. 10. Similar to the results in previous studies using single station records (Yu et al., 2007a; Li et al., 2008), both RRE intensity and frequency occurring in late afternoon (1500–1900 LST) and early morning (0300–0800 LST) dominate the rainfall peaks

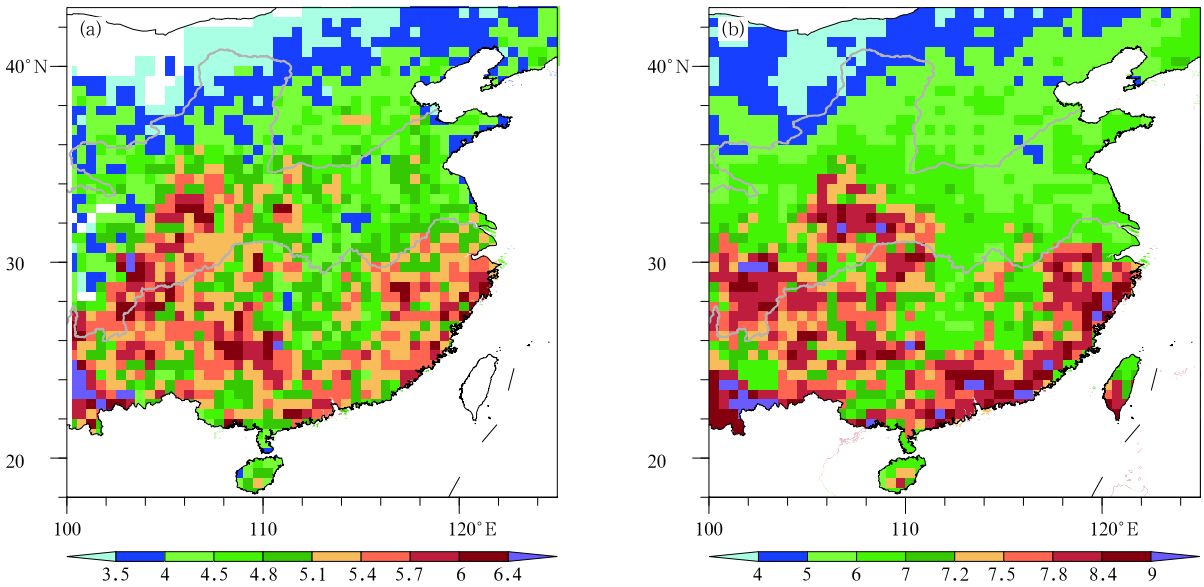


**Fig. 9.** Spatial distributions of 2008–2013 warm-season mean duration (h) of RREs derived from (a) rain gauge observations and (b) CMPA-Hourly data.

over central–eastern China. The two datasets show almost the same results. The RREs lasting shorter than or equal to 9 h primarily show a late-afternoon diurnal peak, and those lasting longer than 12 h mainly present a late-night to early-morning peak. The diurnal amplitude of afternoon short-duration RREs is stronger than that of nocturnal long-duration RREs. Since RREs of long duration (lasting longer than 12 h) are the main contributors to the total rainfall amount (Yu et al., 2007a), and usually have substantial impacts on the regional hydrological cycle and thus severe weather disasters, the diurnal variation of these events, with an intensity larger than 2 mm $h^{-1}$ (hereafter referred to as intense long-duration RREs), is further analyzed.

The diurnal variations of intense long-duration RREs are illustrated in Fig. 11. To fully investigate the diurnal variations, the most frequent hours when these events tend to peak, start, and cease are given separately. The most frequent peak hours are almost the same in station observations (Fig. 11a) and CMPA-Hourly data (Fig. 11b), which, as reported earlier, show differences in their diurnal phases of RRE intensity and frequency (Fig. 6). Along the Yangtze River valley and over the regions between the Yangtze and Yellow rivers, the RRE tends to peak around midnight to the morning hours. Of note is that the eastward delayed diurnal phase along the Yangtze River valley is not so obvious as that when using single station or satellite grids for the analyses (Yu et al., 2007a; Chen et al., 2010; Chen G. X. et al., 2012). The afternoon peak still dominates in the regions over south-

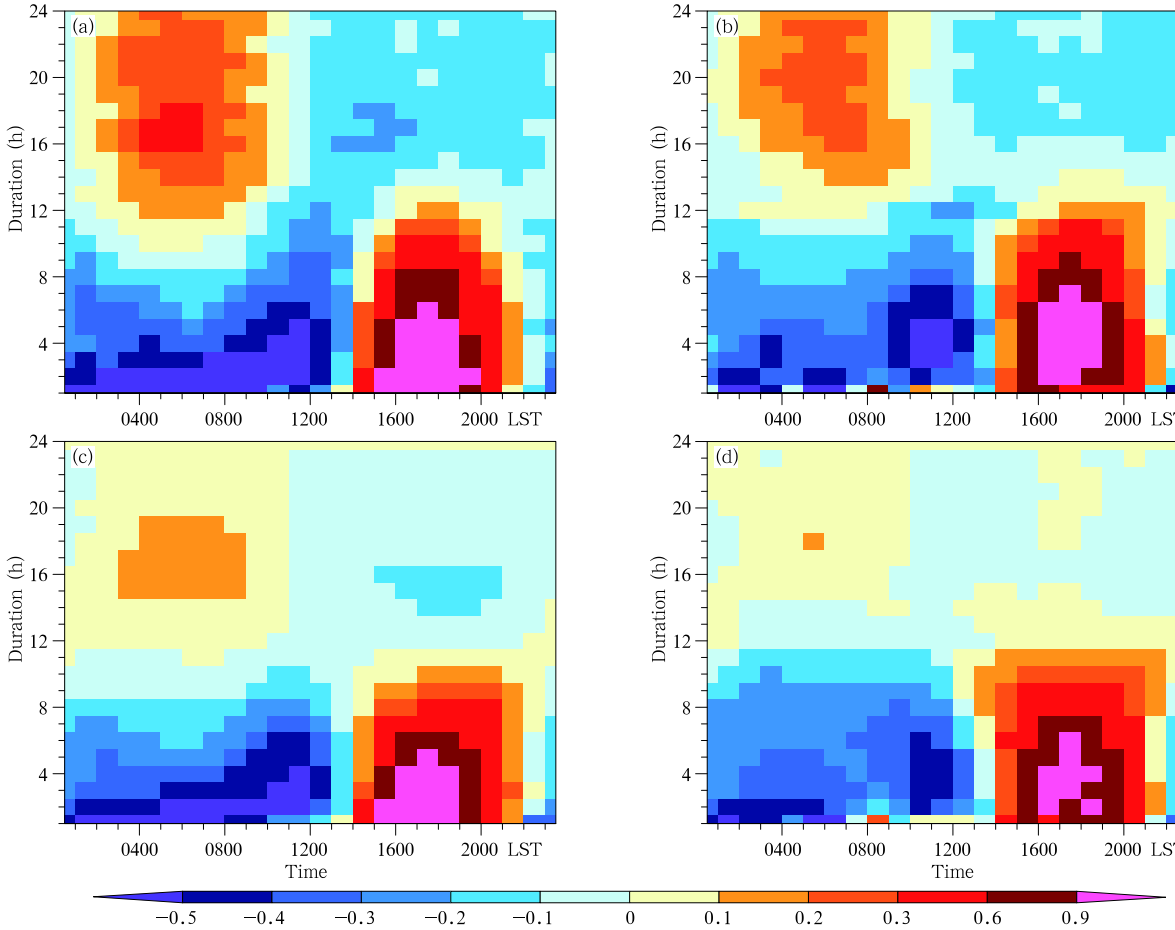


**Fig. 10.** The normalized diurnal variations (normalized by the daily mean) of the warm-season mean hourly (a, b) intensity and (c, d) frequency of RREs with different durations averaged over central–eastern China (18°–43°N, 100°–125°E) from (a, c) rain gauge observations and (b, d) CMPA-Hourly data.

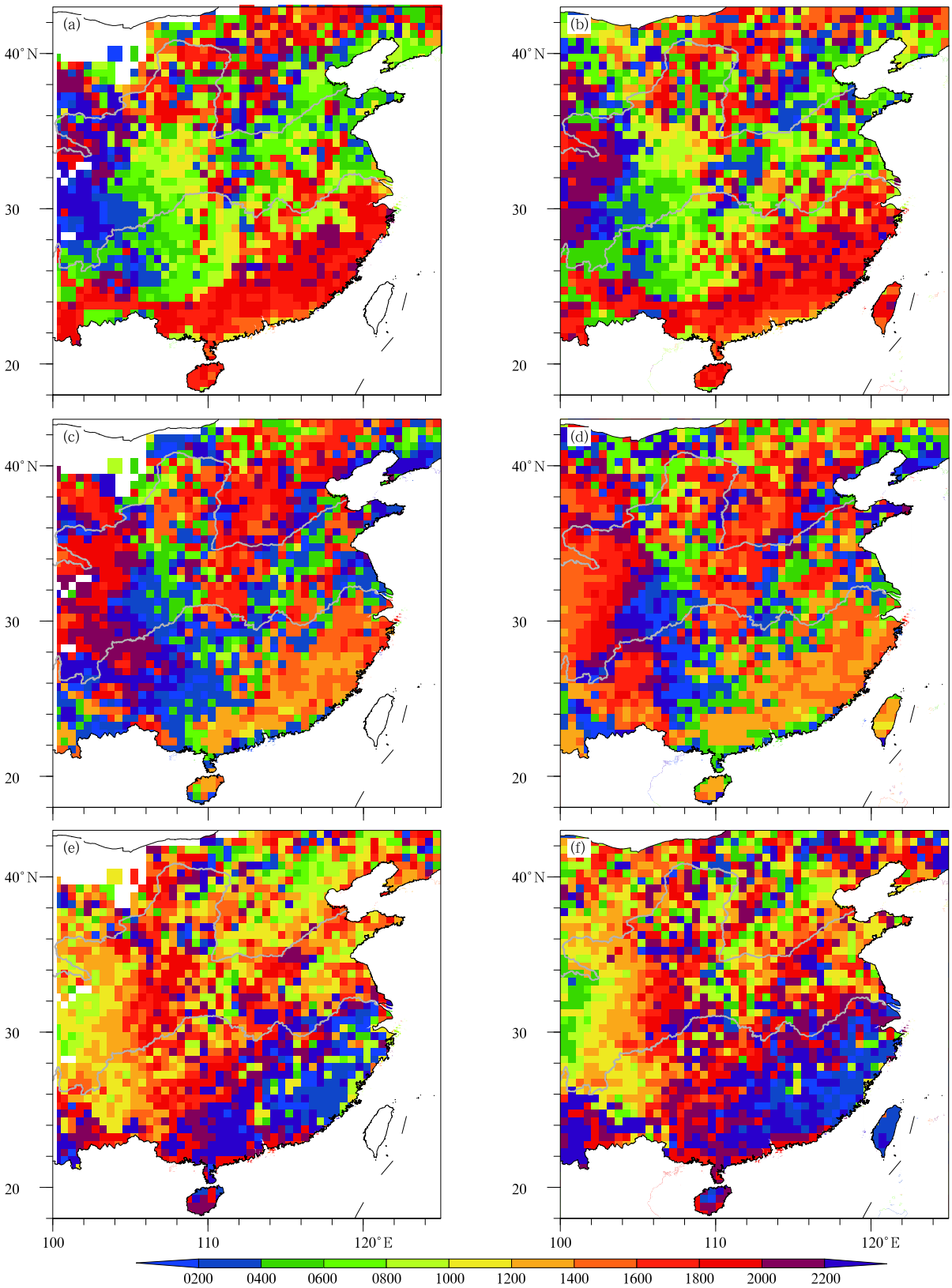


**Fig. 11.** Spatial distributions of the most frequent hours when intense long-duration RREs (a, b) peak, (c, d) start, and (e, f) cease, based on (a, c, e) rain gauge observations and (b, d, f) CMPA-Hourly data. The different colors represent different hours.

eastern China. Over northern China, the afternoon and nocturnal peaks are comparable. The usual start and cease hours are also consistent between the two datasets. Over southeastern and northern China, the intense long-duration RREs tend to start in the afternoon and cease around midnight to morning. The usual start hours are earlier over southeastern regions than those in northern regions, and the cease hours show the same trend. For example, over southeastern China, intense long-duration RREs tend to start during 1200–1400 LST and cease during 2200–0200 LST; while over northern China, these events start more frequently during 1600–2000 LST and cease during 0800–1200 LST. Over the Sichuan basin, intense long-duration RREs tend to start around midnight and cease in the afternoon. Over the regions between the Yangtze and Yellow rivers, the usual start and cease hours show no evident regional consistency.

## 5. Summary and concluding remarks

This study employs the newly defined RRE concept of Yu et al. (2015) as a new metric to compare merged precipitation analysis and satellite precipitation products with rain gauge observations. The comparison provides a reference for the reliability of satellite products on the sub-daily scale over central–eastern China, and the results should prove helpful in understanding the evolution of, and mechanisms behind, rainfall characteristics over the East Asian monsoon regions. The major conclusions can be summarized as follows.

(1) By investigating hourly rainfall characteristics from a regional perspective, the warm-season mean frequency and intensity of RREs in different precipitation datasets show similar distributions over most of central–eastern China. The commonly recognized overestimation (underestimation) of frequency (intensity) in satellite-based products is largely eliminated.

(2) The diurnal variations of RRE intensity and frequency are also comparable among different datasets. The overestimation of the afternoon peak is not obvious in both TRMM and CMORPH, but the RRC reaches a diurnal maximum more frequently in the afternoon in TRMM and CMORPH than in gauge and CMPA-Hourly data.

(3) Despite the similarities among different datasets, the CMPA-Hourly data show considerable advantages in reproducing the gauge-observed mean state and diurnal variation of RRE, as compared with the TRMM and CMORPH datasets, over central–eastern China.

The CMPA-Hourly dataset is more consistent with station observations because it is constructed based on a combination of station and satellite observations. Nonetheless, we also found some differences between gauge observations and CMPA-Hourly data. As CMPA-Hourly is also a gridded product, it is somewhat biased to compare its reliability with rain gauges at a fixed location. This is why we argue that it should be more appropriate to compare different products from an RRE perspective. From our results, CMPA-Hourly is comparable with station observations over the regions with a dense station network; only a small number of differences are found, which may be introduced by interpolation. However, over the regions with a sparse network, e.g., over the eastern slope of the Tibetan Plateau, with its steep topography, these two datasets still show some differences on the sub-daily timescale. The frequency and intensity of RREs, as well as the RRC, in CMPA-Hourly are closer to those in satellite-based products.

By applying this newly defined RRE concept of Yu et al. (2015), this study compares hourly characteristics of rainfall events in a limited region over central–eastern China. It is found that the commonly recognized overestimation of afternoon rainfall in satellite products can be largely due to the comparison method employed. Since rain gauges only observe rainfall at one fixed location, while satellite instruments estimate the rainfall as an average over a grid box, it is not reasonable to compare them at the station location or simply average to the same resolution. These two kinds of data usually show more consistency in representing rainfall in the nocturnal to morning hours because such events are always related to large-scale systems and tend to spread more uniformly in spatial terms, being more easily captured by both in-situ

observations and grid estimates. However, in the afternoon, when local thermal convection on small scales is more active, rainfall systems can be small, and the ability to capture these local systems differs among different measurement methods. Nevertheless, if the rainfall features in a limited region are considered as a whole, the discrepancy should be largely reduced.

The method proposed in this study also provides a more reasonable way to evaluate simulated rainfall features in numerical models. In the last decade or so, the meteorological community has become increasingly concerned with the uncertainty in model verification results arising from many sources (Jolliffe, 2007; Gilleland et al., 2010). Previous work argues that observations are inherently uncertain due to measurement as well as spatial and temporal representativeness errors, and the application of model verification to limited samples of forecasts leads to uncertainty related to sampling variability (Ciach and Krajewski, 1999; Bowler, 2008). As precipitation is produced by sub-grid-scale physics averaged to the model grid, the results could differ compared to those obtained from rain gauge observations or remote sensing measurements. However, the rainfall produced by the model should be able to represent regional-scale rainfall characteristics, and thus evaluation using RREs could provide more useful information on the advantages and deviations of a particular model. Furthermore, the rainfall produced by models with different horizontal resolutions represents systems of different scales; the application of this method in model evaluation and its usability in evaluating models with different resolutions still needs further study.

## REFERENCES


Bao, X. H., and F. Q. Zhang, 2013: Impacts of the mountain-plain solenoid and cold pool dynamics on the diurnal variation of warm-season precipitation over northern China. *Atmos. Chem. Phys.*, **13**, 6965–6982.

Bhatt, B. C., and K. Nakamura, 2005: Characteristics of monsoon rainfall around the Himalayas revealed by TRMM precipitation radar. *Mon. Wea. Rev.*, **133**, 149–165.

Bowler, N. E., 2008: Accounting for the effect of observation errors on verification of MOGREPS. *Meteor. Appl.*, **15**, 199–205.

Bowman, K. P., J. C. Collier, G. R. North, et al., 2005: Diurnal cycle of tropical precipitation in tropical rainfall measuring mission (TRMM) satellite and ocean buoy rain gauge data. *J. Geophys. Res.*, **110**, D21104.

Carbone, R. E., J. D. Tuttle, D. A. Ahijevych, et al., 2002: Inferences of predictability associated with warm season precipitation episodes. *J. Atmos. Sci.*, **59**, 2033–2056.

Chen, G. X., W. M. Sha, T. Iwasaki, et al., 2012: Diurnal variation of rainfall in the Yangtze River valley during the spring–summer transition from TRMM measurements. *J. Geophys. Res.*, **117**, D06106.

Chen, G. X., W. M. Sawada, M. Sawada, et al., 2013: Influence of summer monsoon diurnal cycle on moisture transport and precipitation over eastern China. *J. Geophys. Res.*, **118**, 3163–3177.

Chen, H. M., R. C. Yu, J. Li, et al., 2010: Why nocturnal long-duration rainfall presents an eastward-delayed diurnal phase of rainfall down the Yangtze River valley. *J. Climate*, **23**, 905–917.

Chen Haoming, Yuan Weihua, Li Jian, et al., 2012: A possible cause for different diurnal variations of warm season rainfall as shown in station observations and TRMM 3B42 data over the southeastern Tibetan Plateau. *Adv. Atmos. Sci.*, **29**, 193–200.

Chen Jiong, Zheng Yongguang, Zhang Xiaoling, et al., 2013: Distribution and diurnal variation of warm-season short-duration heavy rainfall in relation to the MCSs in China. *Acta Meteor. Sinica*, **27**, 868–888.

Ciach, G. J., 2003: Local random errors in tipping-bucket rain gauge measurements. *J. Atmos. Oceanic Technol.*, **20**, 752–759.

Ciach, G. J., and W. F. Krajewski, 1999: On the estimation of radar rainfall error variance. *Adv. Water Resourc.*, **22**, 585–595.

Dai, A. G., F. Giorgi, and K. E. Trenberth, 1999: Observed and model-simulated diurnal cycles of precipitation over the contiguous United States. *J. Geophys. Res.*, **104**, 6377–6402.

Dai, A. G., X. Lin, and K.-L. Hsu, 2007: The frequency, intensity, and diurnal cycle of precipitation in surface and satellite observations over low and mid latitudes. *Climate Dyn.*, **29**, 727–744.

Gilleland, E., D. A. Ahijevych, B. G. Brown, et al., 2010: Verifying forecasts spatially. *Bull. Amer. Meteor. Soc.*, **91**, 1365–1373.

Guo, J. P., P. M. Zhai, L. Wu, et al., 2014: Diurnal variation and the influential factors of precipitation from surface and satellite measurements in Tibet. *Int. J. Climatol.*, **34**, 2940–2956.

Hirose, M., and K. Nakamura, 2005: Spatial and diurnal variation of precipitation systems over Asia observed by the TRMM precipitation radar. *J. Geophys. Res.*, **110**, D05106.

Houze Jr., R. A., 1997: Stratiform precipitation in regions of convection: A meteorological paradox. *Bull. Amer. Meteor. Soc.*, **78**, 2179–2196.

Huffman, G. J., D. T. Bolvin, E. J. Nelkin, et al., 2007: The TRMM multisatellite precipitation analysis (TMPA): Quasi-global, multiyear, combined-sensor precipitation estimates on fine scales. *J. Hydrometeorol.*, **8**, 38–55.

Janowiak, J. E., V. E. Kousky, and R. J. Joyce, 2005: Diurnal cycle of precipitation determined from the CMORPH high spatial and temporal resolution global precipitation analyses. *J. Geophys. Res.*, **110**, D23105.

Jolliffe, I. T., 2007: Uncertainty and inference for verification measures. *Wea. Forecasting*, **22**, 637–650.

Joyce, R. J., J. E. Janowiak, P. A. Arkin, et al., 2004: CMORPH: A method that produces global precipitation estimates from passive microwave and infrared data at high spatial and temporal resolution. *J. Hydrometeorol.*, **5**, 487–503.

Kikuchi, K., and B. Wang, 2008: Diurnal precipitation regimes in the global tropics. *J. Climate*, **21**, 2680–2696.

Li, J., R. C. Yu, and T. J. Zhou, 2008: Seasonal variation of the diurnal cycle of rainfall in the southern contiguous China. *J. Climate*, **21**, 6036–6043.

Li, J., R. C. Yu, W. H. Yuan, et al., 2011: Changes in duration-related characteristics of late-summer precipitation over eastern China in the past 40 years. *J. Climate*, **24**, 5683–5690.

Moron, V., A. W. Robertson, and J.-H. Qian, 2010: Local- versus regional-scale characteristics of monsoon onset and post-onset rainfall over Indonesia. *Climate Dyn.*, **34**, 281–299.

Moseley, C., P. Berg, and J. O. Haerter, 2013: Probing the precipitation life cycle by iterative rain cell tracking. *J. Geophys. Res.*, **118**, 13361–13370.

Nesbitt, S. W., and E. J. Zipser, 2003: The diurnal cycle of rainfall and convective intensity according to three years of TRMM measurements. *J. Climate*, **16**, 1456–1475.

Sapiano, M. R. P., and P. A. Arkin, 2009: An intercomparison and validation of high-resolution satellite precipitation estimates with 3-hourly gauge data. *J. Hydrometeorol.*, **10**, 149–166.

Satoh, M., and Y. Kitao, 2013: Numerical examination of the diurnal variation of summer precipitation over southern China. *SOLA*, **9**, 129–133.

Shen, Y., A. Y. Xiong, Y. Wang, et al., 2010: Performance of high-resolution satellite precipitation products over China. *J. Geophys. Res.*, **115**, D02114.

Shen, Y., P. Zhao, Y. Pan, et al., 2014: A high spatiotemporal gauge-satellite merged precipitation analysis over China. *J. Geophys. Res.*, **119**, 3063–3075.

Soltani, S., and R. Modarres, 2006: Classification of spatio-temporal pattern of rainfall in Iran using a hierarchical and divisive cluster analysis. *J. Spatial Hydrol.*, **6**, 1–12.

Sorooshian, S., X. Gao, K. Hsu, et al., 2002: Diurnal variability of tropical rainfall retrieved from combined GOES and TRMM satellite information. *J. Climate*, **15**, 983–1001.

Tian, Y. D., C. D. Peters-Lidard, and J. B. Eylander, 2010: Real-time bias reduction for satellite-based precipitation estimates. *J. Hydrometeorol.*, **11**, 1275–1285.

Toews, M. W., D. M. Allen, and P. H. Whitfield, 2009: Recharge sensitivity to local and regional precipitation in semiarid midlatitude regions. *Water Resourc. Res.*, **45**, W06404.

Trenberth, K. E., A. G. Dai, R. M. Rasmussen, et al., 2003: The changing character of precipitation. *Bull. Amer. Meteor. Soc.*, **84**, 1205–1217.

Wallace, J. M., 1975: Diurnal variations in precipitation and thunderstorm frequency over the conterminous United States. *Mon. Wea. Rev.*, **103**, 406–419.

Xu, W. X., 2013: Precipitation and convective characteristics of summer deep convection over East Asia observed by TRMM. *Mon. Wea. Rev.*, **141**, 1577–1592.

Yang, G. Y., and J. Slingo, 2001: The diurnal cycle in the tropics. *Mon. Wea. Rev.*, **129**, 784–801.

Yu, R. C., Y. P. Xu, T. J. Zhou, et al., 2007a: Relation between rainfall duration and diurnal variation in the warm season precipitation over central eastern China. *Geophys. Res. Lett.*, **34**, L13703.

Yu, R. C., T. J. Zhou, A. Y. Xiong, et al., 2007b: Diurnal variations of summer precipitation over contiguous China. *Geophys. Res. Lett.*, **34**, L01704.

Yu, R. C., J. Li, W. H. Yuan, et al., 2010: Changes in characteristics of late-summer precipitation over eastern China in the past 40 years revealed by hourly precipitation data. *J. Climate*, **23**, 3390–3396.

Yu, R. C., and J. Li, 2012: Hourly rainfall changes in response to surface air temperature over eastern contiguous China. *J. Climate*, **25**, 6851–6861.

Yu, R. C., H. M. Chen, and W. Sun, 2015: The definition and characteristics of regional rainfall events demonstrated by warm season precipitation over the Beijing Plain. *J. Hydrometeorol.*, **16**, 396–406.

Yuan, W. H., R. C. Yu, H. M. Chen, et al., 2010: Subseasonal characteristics of diurnal variation in summer monsoon rainfall over central eastern China. *J. Climate*, **23**, 6684–6695.

Yuan, W. H., J. Li, H. M. Chen, et al., 2012: Intercomparison of summer rainfall diurnal features between station rain gauge data and TRMM 3b42 product over central eastern China. *Int. J. Climatol.*, **32**, 1690–1696.

Zhang Huan and Zhai Panmao, 2011: Temporal and spatial characteristics of extreme hourly precipitation over eastern China in the warm season. *Adv. Atmos. Sci.*, **25**, 1177–1183.

Zhou, T. J., R. C. Yu, H. M. Chen, et al., 2008: Summer precipitation frequency, intensity, and diurnal cycle over China: A comparison of satellite data with rain gauge observations. *J. Climate*, **21**, 3997–4010.